RSC Advances

PAPER

View Article Online
View Journal | View Issue

Cite this: *RSC Adv.*, 2019, **9**, 24802

A thin film nanocomposite membrane with pre-immobilized UiO-66-NH_2 toward enhanced nanofiltration performance†

Xu Zhang,‡[a] Yufan Zhang,‡[b] Tiecheng Wang,[a] Zheng Fan[a] and Guoliang Zhang *[a]

A facile controlled interfacial polymerization strategy was proposed for the synthesis of novel thin film nanocomposite (TFN) membranes for enhanced nanofiltration performance. UiO-66 nanoparticles were aminated and pre-immobilized onto a polymer substrate *via* polydopamine (PDA) coating to achieve a continuous and defect-free polyamide dense layer. The mediation of the PDA coating could not only enhance the structural stability of TFN nanofiltration membranes, but also improve the dispersion and anchorage of UiO-66-NH_2, thus closely fixing the position of UiO-66-NH_2 nanoparticles on the polymer substrate. Moreover, since the amino group (–NH_2) further reacted with PDA *via* Michael addition or Schiff base reaction, the *in situ* mutual reaction reduced the nanoparticle losses significantly during the draining off of the monomer solution in the fabrication process, which effectively cut down the actual dosage. The results showed that the PDA interlayer could induce the tight attachment of the PA layer to the support, enhancing the structural stability of TFN membranes. Furthermore, the dosage of UiO-66-NH_2 in the as-prepared TFN membranes could also be decreased to as low as 0.01 w/v%, which was nearly a 10–20-fold reduction in the required amount of UiO-66-NH_2 for the synthesis. The fabricated TFN/UiO-66-NH_2 membranes exhibited very high water permeance and competitive salt rejections in cross-flow nanofiltration, which shows the huge potential for the application of novel TFN membranes with controlled nanoparticle incorporation in industrial separation.

Received 23rd June 2019
Accepted 25th July 2019

DOI: 10.1039/c9ra04714j

rsc.li/rsc-advances

Introduction

With the depletion of water resources and the increase in water consumption, advanced separation methods for improving efficient water usage are imperative. Among various strategies, membrane separation technologies are gaining worldwide attention.[1,2] As a typical and most important technique, nanofiltration (NF) presents excellent rejection capability of multivalent ions and low-molecular-weight organics,[3] and has been widely applied in water treatment processes, including dye separation,[4,5] heavy metal removal[6,7] and desalination.[8,9] Currently, most of the NF membranes are fabricated through interfacial polymerization between diamine aqueous and organic solutions containing acylchoride to constitute thin film composite (TFC) membranes.[10] However, these membranes are typically subjected to the permeation–rejection trade-off, restricting their tremendous applications in industry.[11]

To address this issue, incorporating nanofillers such as silica,[12] TiO_2,[13] carbon nanotubes,[14] graphene[15] and metal–organic frameworks (MOFs)[16] into a polyamide (PA) active layer to prepare thin-film nanocomposite (TFN) membranes is likely to be an efficacious method. The introduction of nanoparticles provides additional pathways to enhance mass transfer within the selective layer *via* their intrinsic nanosized pores and interface voids, which maintain the original molecular sieving capacity of membranes. Unlike stiff inorganic materials, MOFs have attracted much attention in TFN membranes because of their singularly accessible surface area, large pore volumes, and flexible and tunable pore structures.[17–19] The preparation of MOF-based mixed matrix membranes, which are similar to other nanofillers, provides a useful approach to improve their processability.[20] However, the binding between MOFs and polymer substrates usually presents poor compatibility due to the easy aggregation of MOF nanoparticles, leading to a significant decrease in membrane separation performance. Moreover, as numerous expensive MOFs are unavoidably wasted during interfacial polymerization, only a small amount of nanofillers are left behind and incorporated into the PA dense layer, which severely hinder their potential effects. To cut down the usage of MOFs, volatile solvents are always used, which will

[a]*Institute of Oceanic and Environmental Chemical Engineering, State Key Lab Breeding Base of Green Chemical Synthesis Technology, Zhejiang University of Technology, Chaowang Road 18#, 310014 Hangzhou, P. R. China. E-mail: guoliangz@zjut.edu.cn*
[b]*Department of Mechanical Engineering, College of Engineering, Carnegie Mellon University, Pittsburgh, PA 15213, USA*

† Electronic supplementary information (ESI) available: XRD pattern, SEM images, and the data for the gas separation. See DOI: 10.1039/c9ra04714j

‡ These authors contributed equally.

increase environmental burdens.[20,21] Therefore, in order to fabricate high-quality TFN MOF membranes, new materials and environment-friendly methods are urgently needed to offer preferable affinity with polymer binders as well as an effective control over the incorporation to minimize the loss in amount of costly MOFs.

As a prototype Zr-MOF, UiO-66 has displayed interesting physical and chemical characteristics for the preparation of highly water-stable MOF membranes for liquid separation.[22–24] The highly regular structure of UiO-66 with the aperture size of about 6.0 Å,[25,26] which is located between H_2O (2.6 Å) and hydrated ions (*e.g.* Na^+ 7.2 Å, Mg^{2+} 8.6 Å, SO_4^{2-} 7.6 Å, Cl^- 6.6 Å), is promising for achieving high flux and sustains high salt rejections by ionic sieving. As important analogues, aminated UiO-66 (UiO-66-NH_2) was synthesized by substituting 2-aminoterephthalic acid for terephthalic acid. The free amino groups of UiO-66-NH_2 nanoparticles enable surface-modification with other chemical compounds without sacrificing the stability of the parent material, which might provide a good scope for improving the compatibility between MOFs and polymers for fabricating well-dispersed and stable TFN MOF membranes.

To step forward for the precise control of MOF nanoparticle incorporation, a strong relationship between the PA dense layer and polymer substrate should be built. If the nanofillers are tightly combined with the substrate, they will not easily leach during pouring off of the monomer solution. However, the commonly used substrates, such as polysulfone (PSF), polyethersulfone and polyacrylonitrile (PAN), could not carry out this goal. Dopamine, an interesting mussel-inspired material from nature,[27] can be applied to modify the support surface and construct a platform to enhance the combination with nanoparticles. As noticed, dopamine can self-polymerize into polydopamine (PDA) in weak alkaline condition with the assistance of oxygen, and form a thin and stable surface coating on different types of material surfaces at ambient temperature.[28,29] Furthermore, PDA coatings can offer a physically and chemically versatile platform for further decoration. The amino group (–NH_2) can further react with PDA *via* Michael addition or Schiff base reaction.[30,31] Thus, based on our understanding, a PDA-modified substrate might be a good choice to apply as the mutual support for the preparation of high-quality TFN MOF membranes.

Taking the aforementioned into consideration, herein, we directly anchored UiO-66-NH_2 nanoparticles onto the polydopamine modified polymer substrates by using a new controlled interfacial polymerization method. High-quality TFN nanofiltration membranes with defect-free PA dense layers can easily be synthesized on a PDA buffering layer with controlled UiO-66-NH_2 incorporation (Fig. 1). Our method may have the following features: (i) the mediation of PDA coating could enhance the structural stability of TFN NF membranes;[32] (ii) UiO-66-NH_2 nanoparticles can be precisely immobilized by the homogeneous coating of PDA, greatly improving the dispersion and anchorage of UiO-66-NH_2; (iii) the mutual reaction can significantly reduce the nanoparticle losses during the draining off of the monomer solution, thus effectively cutting down the actual dosage and reducing environmental impact. To the best of our knowledge, so far, there is no report on fabricating a TFN membrane *via* pre-immobilized nanofillers onto the polymer substrate. Moreover, based on the mechanism of this method, we can prepare various TFN membranes with amino-containing particles as nanofillers on versatile polymer substrates.

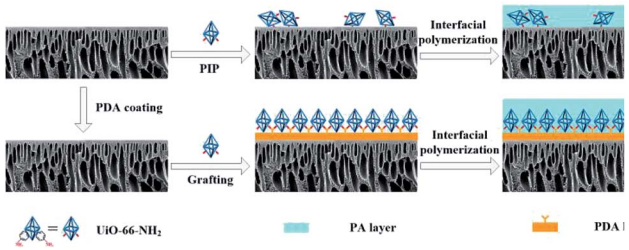

Fig. 1 Schematic of the synthesized TFN/UiO-66-NH_2 membrane.

Experimental section

Materials

Polysulfone (PSF) powders were purchased from Changzheng Chemical Reagent Co., Ltd (China) and dried for at least 12 h at 80 °C before use. Zirconium(IV) chloride ($ZrCl_4$, 98%), 2-aminoterephthalic acid (ATA), L-dopamine, and 1,3,5-benzenetricarbonyl trichloride (TMC) were provided by Aladdin Chemistry Co., Ltd (China). Inorganic salts, namely, sodium chloride (NaCl), sodium sulfate (Na_2SO_4), magnesium chloride ($MgCl_2$), and magnesium sulfate ($MgSO_4$) as well as *N*,*N*-dimethylformamide (DMF), piperazine (PIP), acetic acid, methanol, hydrochloric acid solution (18 mol L^{-1}) and *n*-hexane were bought from Sinopharm Chemical Reagent Co., Ltd (China). Tris(hydroxymethyl)aminomethane (Tris) was procured from Shanghai Bo'ao Biological Technology Co., Ltd (China). Deionized (DI) water used in the studies was produced by a nanofiltration-reverse osmosis (RO-EDI) system, and the ion concentration was matched with the experimental requirement of $\sigma \leq 0.5$ μs cm^{-1}. All the chemicals were of analytical grade unless specified, and were used as received without further purification.

Synthesis of UiO-66-NH_2 nanoparticles

UiO-66-NH_2 nanoparticles were synthesized through a solvothermal reaction with a slight modification by adding a certain amount of acetic acid.[25] In detail, 0.305 g of $ZrCl_4$ and 0.215 g of ATA were added in 75 mL DMF, followed by the addition of 2.235 mL acetic acid. The mixed solution was then transferred into a Teflon-lined stainless steel autoclave (100 mL) and heated at 120 °C for 24 h. After cooling to ambient temperature, the solution was centrifuged (10 min, 8000 rpm) to obtain yellow UiO-66-NH_2 powder. The product was washed with methanol and then dried for 12 h at 60 °C.

PSF membrane substrates preparation and modification

Polysulfone (PSF) membrane substrates were fabricated *via* a phase inversion method. In this process, dried PSF powders

were dissolved into DMF (12 wt% PSF, 88 wt% DMF) and stirred at room temperature for 12 h. The obtained homogeneous and uniform casting suspension solution was sonicated for degasification. Subsequently, the solution was cast over a glass plate using a casting knife of 200 μm height, and then immediately put into a DI water coagulation bath at room temperature for phase inversion. To remove the remaining solvent, the prepared substrates were kept in DI water overnight. All membranes were stored in deionized water before use. L-Dopa (2 g L^{-1}) was added into Tris–HCl buffer solution (pH = 8.5, 10 mmol L^{-1}) to form a dopamine coating solution. The PSF membranes were transferred into the aforementioned solution and shaken at ambient temperature for a certain amount of time (from 3 to 24 h). Following this, the polydopamine (PDA) deposited PSF substrates were washed with deionized water thoroughly and named PSF/PDA, and stored in deionized water until use. UiO-66-NH_2 nanoparticles were uniformly dispersed into Tris–HCl buffer solution *via* sonication to obtain a 0.01 w/v% UiO-66-NH_2 solution. Then, the PSF/PDA membranes were immersed into the UiO-66-NH_2 suspended solution to deposit at room temperature for 24 h.

Preparation of TFC, PA/UiO-66-NH_2 and TFN/UiO-66-NH_2 membranes

Typically, the polyamide (PA) dense layer was prepared *via* the interfacial polymerization (IP) method. In the present study, the aqueous phase (2.0% (w/v)) was prepared by dissolving PIP in DI water, and the organic phase (0.1% (w/v)) was produced by dissolving TMC in *n*-hexane. The PSF- or UiO-66-NH_2/PDA@PSF-supported membranes was fixed to a glass substrate for the IP reaction. The as-synthesized aqueous solution was poured onto the supported membrane and left undisturbed for 2 min, and the as-synthesized organic phase was poured to cover the supported membrane for 1 min after draining off the excess water in air. The resultant TFC or TFN/UiO-66-NH_2 membrane was placed in the air for 2 min to evaporate the excess *n*-hexane, and subsequently dried at 80 °C for 5 min before storing in DI water. For comparison, PA/UiO-66-NH_2 was prepared on the surface of pure PES by blending UiO-66-NH_2 into PIP solution (0.01 w/v%) during interfacial polymerization.

Membrane filtration test

Separation performances of pure TFC and TFN/UiO-66-NH_2 membranes were tested by measuring pure water permeability (PWP) and salt rejection. The experiment was carried out in a self-made cross-flow filtration system (Fig. 2), similar to our previous study. The effective area of the membrane was 7.065 cm^2. The membrane was pre-pressurized for 30 min at 0.6 MPa until the PWP of the membrane reached a steady state. The PWP of the as-synthesized membranes was calculated on the basis of the following eqn (1):

$$\mathrm{PWP} = \frac{Q}{A \times \Delta P} \quad (1)$$

where PWP is the permeation flux (L m^{-2} h^{-1} bar^{-1}), t is the permeation time (h), Q represents the water flux at the permeate side (L h^{-1}) and A is the effective membrane area (m^2), and ΔP is the transmembrane pressure (bar).

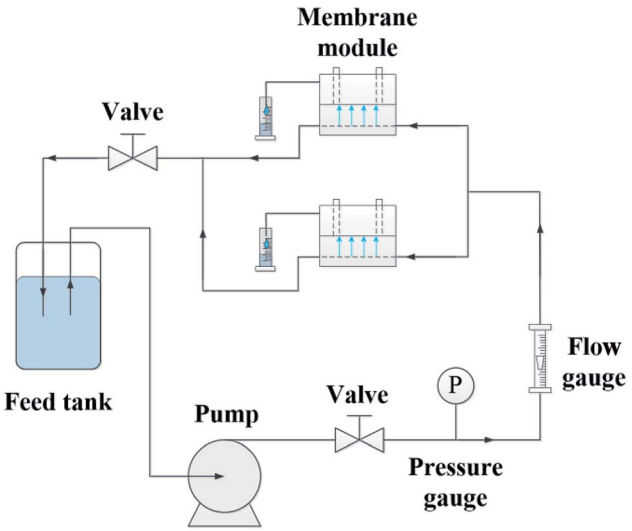

Fig. 2 Schematic of the synthesized TFN/UiO-66-NH_2 membrane.

After the PWP tests, feed solutions containing 1000 ppm concentrations of either NaCl, $MgCl_2$, Na_2SO_4, or $MgSO_4$ were used to assess the water permselective performance of these TFN/UiO-66-NH_2 membranes. The rejection (R) of each NF membrane was calculated by using formula (2):

$$R\ (\%) = \left(1 - \frac{C_p}{C_f}\right) \times 100 \quad (2)$$

where C_p represents the concentration of permeate solution and C_f represents the concentration of feed solution.

Characterization

All samples containing the UiO-66-NH_2 and fabricated membranes were characterized after being dried. Powder X-ray diffraction (XRD) analysis of the UiO-66-NH_2 nanoparticles was analyzed by an X'Pert PRO X-ray diffractometer with Cu Kα radiation source (λ = 1.5418 Å). The morphologies of the UiO-66-NH_2 nanoparticles and membranes were inspected by using Hitachi S-4800 scanning electric microscopy (SEM). The chemical structures of the UiO-66-NH_2 nanoparticles and as-prepared membranes were investigated by Fourier transform infrared (FTIR) spectroscopy using a Nicolet 6700 FTIR spectrometer. The surface chemical compositions of the membranes were measured by a X-ray photoelectron spectroscopy (RAD upgraded PHI-5000C ESCA system (PerkinElmer)) using Mg Kα as the radiation source. The elemental composition of membranes was analysed by energy-dispersive X-ray spectroscopy (EDX, HIYACHI SU8010, JPN). To study the surface wettability of the membranes, pure water contact angles (WCA) of the surfaces of the TFC and TFN/UiO-66-NH_2 membranes were determined using a Dataphysics OCA20 (Germany) contact angle goniometer under ambient conditions, and at least three measurement were carried out to get an average value of the WCA for each membrane.

Stability of UiO-66-NH_2 nanoparticles on the membrane

The poor adhesion and compatibility between nanofillers and PA layer is one of the primary issues obstructing the practical application of TFN membranes, and the leaching out of the nanofillers is an important index. To determine the amount of UiO-66-NH_2 nanoparticles leaching out from the membrane, a batch experiment was used to measure the release of Zr ions from PA/UiO-66-NH_2 membrane and TFN/UiO-66-NH_2 membrane. First, a membrane specimen with an area of 9 cm^2 was dipped in 40 mL DI water in a container. Following this, the batch container was subjected to shaking in incubator at 130 rpm for 24 h. Finally, the water samples were analyzed for the presence of Zr ions by an IRIS Intrepid ICP.

Results and discussion

The micro-morphologies of UiO-66-NH_2 nanoparticles were characterized by SEM. As shown in Fig. 3a, they are octahedrally cubic nanocrystals, similar to those reported in literature.[23] As shown in Fig. 3b, the particle sizes of UiO-66-NH_2 range from 65 to 150 nm. In addition, 70% of these have size below 110 nm and the average size was 98 nm. The powder XRD pattern of the as-resulted UiO-66-NH_2 nanoparticles is shown in Fig. 3c. Sharp diffraction peaks at $2\theta = 7.4°$, 8.5° and 25.7° were observed in the XRD pattern, owing to (1 1 1), (2 0 0) and (6 0 0) crystal planes, respectively. In addition, the diffraction line of the UiO-66-NH_2 powders well coincided with the value in the previous report,[24] confirming that the MOF particles were successfully synthesized. The chemical structure of the UiO-66-NH_2 nanoparticles was also analyzed by FTIR spectroscopy (Fig. 3d). The adsorption bands from 1385 to 1600 cm^{-1} can be attributed to the characteristic peaks of UiO-66-NH_2. Since the ligand of UiO-66-NH_2 was 2-aminoterephthalic acid, it should contain aromatic carboxylates. Thus, the different peaks at 1423 cm^{-1} can be associated with the C–C vibrational bond, and the peaks at 1385 and 1573 cm^{-1} are assigned to symmetric and asymmetric C–O stretching bonds, respectively, resulting from aromatic and carboxylic groups. Two characteristic peaks at 3518 and 3337 cm^{-1} are derived from the asymmetric and symmetric vibrational bands of the primary amine group, respectively. Moreover, the bonding between aromatic carbon and nitrogen (C–N) could be observed at 1258 and 1338 cm^{-1}, and the peak at 1619 cm^{-1} can be assigned as the bending vibration of N–H. The characteristic peaks at 768 cm^{-1} can be attributed to the Zr–O stretching vibration.[24]

The PSF substrates were first modified with PDA coating, which offer a platform for grafting UiO-66-NH_2 nanoparticles onto the surface of the ultrafiltration membrane. After PDA modification, a dark bark surface was obtained, and the color became darker with the increase in time of deposition reaction. In addition, a porous network structure formed on the support surface (Fig. S1†). Since the compounds containing amino groups can react with PDA through Michael addition or Schiff base reaction in weak alkaline conditions, UiO-66-NH_2 nanoparticles were favourably anchored onto the surface of the PDA@PSF membrane (Fig. 4). To confirm the effect of PDA coating, pure PSF substrate was immersed in 0.01 w/v% UiO-66-NH_2 aqueous solution for 2 min and dried at room temperature. The treatments were similar to those for the typical fabrication of TFN MOF membranes. From Fig. 4, we can find that the loading amount of UiO-66-NH_2 nanoparticles on the pure PSF membrane was much less than that on the UiO-66-NH_2/PDA@PSF membrane. Moreover, UiO-66-NH_2 nanoparticles on the surface of the PSF membrane were more likely to agglomerate than PDA modified supports. All of these observations indicated that the PDA coating provided more reactive sites and increased the loading amount of UiO-66-NH_2. To further confirm the effect of PDA, FTIR was implemented to analyze the chemical structure of the PSF membrane and UiO-66-NH_2/PDA@PSF membrane (Fig. 5). The UiO-66-NH_2/PDA@PSF membrane presented a similar FTIR pattern to that of the PSF substrate. Differently, the peaks at 1649 and 1554 cm^{-1} correspond to C–N and N–H vibrations of UiO-66-NH_2/PDA,[33,34] and the characteristic peak of Zr–O mode (at 764 cm^{-1}) can also be

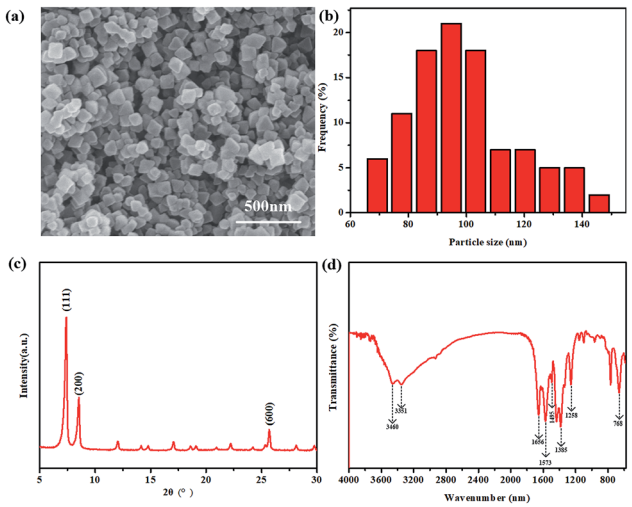

Fig. 3 SEM image (a), size distribution (b), XRD pattern (c) and FTIR (d) of the UiO-66-NH_2 powders.

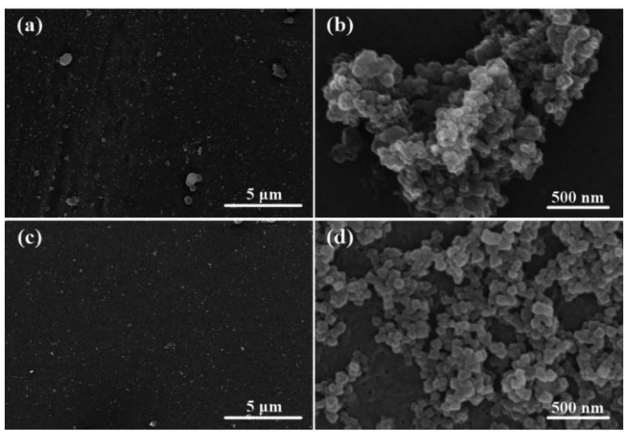

Fig. 4 SEM images of the membrane surfaces of UiO-66-NH_2@PSF (a and b) and UiO-66-NH_2/PDA@PSF (c and d).

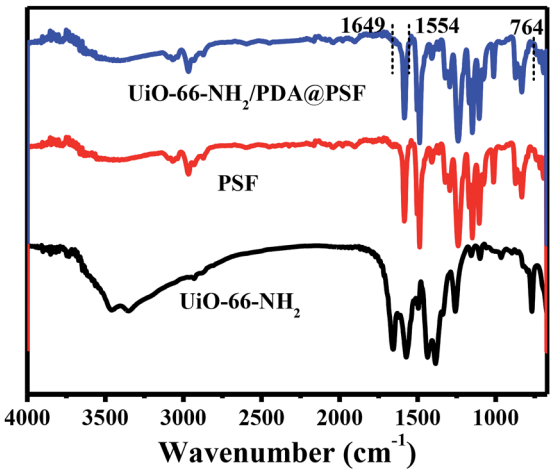

Fig. 5 FTIR spectra of UiO-66-NH_2 powders, PSF, and UiO-66-NH2/PDA @PSF membrane.

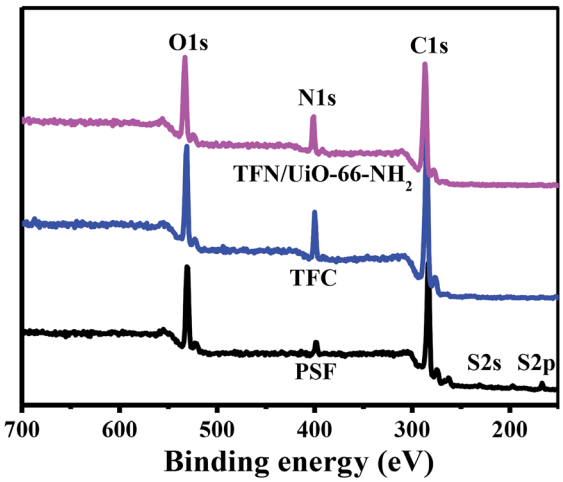

Fig. 7 XPS survey spectra of pristine PSF, TFC, and TFN/UiO-66-NH_2.

observed, demonstrating that PDA coating made the adhesion firmer through strong covalent bonds, and promoted more UiO-66-NH_2 anchoring on the surface of the membrane.

After UiO-66-NH_2 was grafted onto the PSF@PDA membrane successfully, an interfacial polymerization approach of PIP and TMC was carried out for preparing nanofiltration membranes. FTIR was applied to investigate the chemical structures and functional groups of the surfaces of the synthesized TFC and TFN/UiO-66-NH_2 membranes (Fig. 6). The characteristic peaks ascribed to typical PIP-PA structures at 1616 and 1364 cm^{-1} were observed in the FTIR spectra of pure TFC and TFN/UiO-66-NH_2 membranes. These peaks are attributed to the stretching vibration of C=O and stretching vibration of C–N, respectively, indicating that the cross-linked PA structure formed on the substrate surface through interfacial polymerization.[35,36] Fig. 7 shows the XPS survey spectra of pure PSF, TFC and TFN/UiO-66-NH_2 membranes. A new characteristic peak of N 1s was observed in the XPS spectra of TFC and TFN/UiO-66-NH_2 membranes, owing to the formation of dense PA layers. However, the characteristic peaks of S 2s and S 2p faded away in the spectra of TFC and TFN/UiO-66-NH_2 membranes. Furthermore, the characteristic peak of Zr in the XPS survey spectrum of TFN/UiO-66-NH_2 was absent. These results presented that the surfaces of PSF and the UiO-66-NH_2/PDA@PSF membrane were thoroughly enveloped by dense PA layers.

To study the influence of UiO-66-NH_2 nanofillers on the surface morphology of the dense polyamide layer, the morphology of the top surface and cross-section of TFN/UiO-66-NH_2 and PA/UiO-66-NH_2 nanofiltration membranes was characterized by SEM (Fig. 8). For comparison, PA/UiO-66-NH_2 was prepared by blending UiO-66-NH_2 into PIP solution (0.01 w/v%) during interfacial polymerization. The TFC membrane with PSF membrane as support and PA membrane with PDA@PSF as substrate exhibited the typical nodular structure of the PA membrane prepared through interfacial polymerization

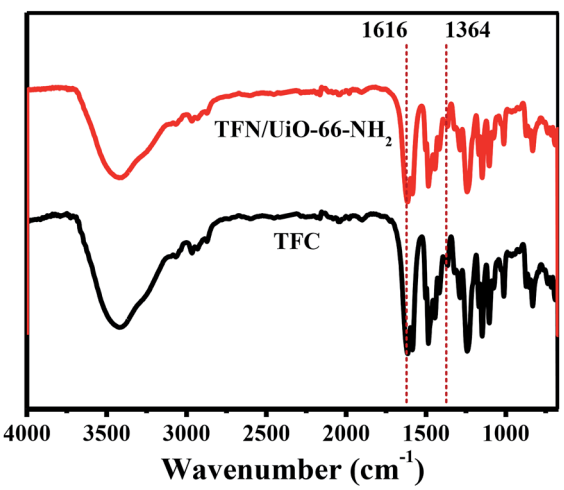

Fig. 6 FTIR spectra of TFC and TFN/UiO-66-NH_2 membranes.

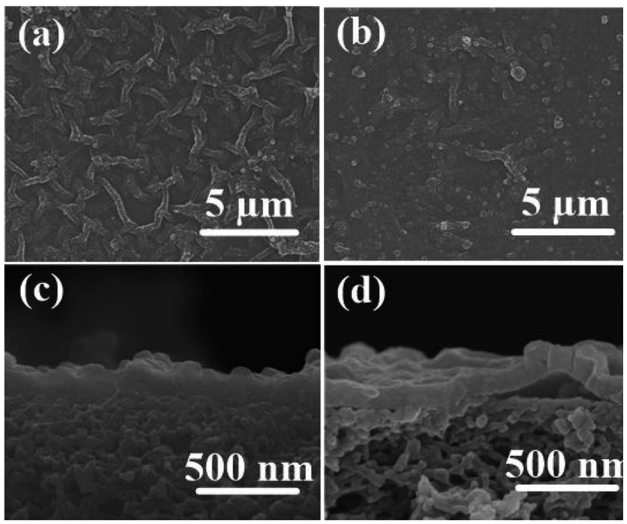

Fig. 8 SEM images of surface and cross-section of TFN/UiO-66-NH_2 membrane (a and c) and PA/UiO-66-NH_2 membrane (b and d).

(Fig. S2†). The dense and rough structure stacked by spherical globules dispersed well on the surface of the PSF substrate, which was formed by cross-linking PIP and TMC.[8] Compared with the pure TFC membrane, TFN/UiO-66-NH_2 membranes have rougher surfaces with apparently denser and bigger nodular-like structures on the UiO-66-NH_2/PDA@PSF substrate (Fig. 8a). Further, these structures can be controlled and strengthened by increasing the PDA deposition time (Fig. S3†). The increase in PDA deposition offered more active sites and improved loading amount of UiO-66-NH_2 nanoparticles. The hydrophilic UiO-66-NH_2 nanoparticles can adsorb more PIP monomers on the surface, resulting in an increase in PIP concentration around UiO-66-NH_2 nanoparticles on the surface of substrate, and not merely into the pores below its surface. Once UiO-66-NH_2/PDA@PSF membranes containing PIP solution were immersed in TMC solution, the outer PIP monomers of the UiO-66-NH_2 nanoparticles first contacted with TMC to form small nuclei of PA above the pore, and further evolved into PA tufts around the UiO-66-NH_2 nanoparticles. Furthermore, the PIP from the inner pores of the substrate could diffuse continuously and react with TMC to form a film, which was crosslinked with the scattered PA tufts.[16] Because the growth orientations of PA tufts and the diffusion trend of PIP were different, a rougher surface structure was formed. As the amount of UiO-66-NH_2 nanoparticles increased, more PIP monomers were absorbed on the surface of the support and thus, the rougher surface with a larger nodular-like structure became more obvious. Compared with the TFN/UiO-66-NH_2 membranes, however, the surface of the PA/UiO-66-NH_2 membrane is relatively smooth; only a few segments showed the larger nodular-like structure. This manifested that the strategy of pre-immobilizing MOFs can enable controlled interfacial polymerization and form a more regular PA structure. As shown in Fig. 8c and d, the cross-sectional SEM images of TFN/UiO-66-NH_2 and PA/UiO-66-NH_2 membranes display the typical structure of a polyamide dense layer and their thicknesses are about 130 nm and 110 nm, respectively. Unlike TFN/UiO-66-NH_2 and TFC membranes, the PA dense layer of the PA/UiO-66-NH_2 membrane displayed poor compatibility with the PSF substrate and may detach from the support. EDX analysis was applied to investigate the elemental composition of the cross-section of the TFN/UiO-66-NH_2 membrane and PA/UiO-66-NH_2 membrane (Fig. S4†). The Zr content in the TFN/UiO-66-NH_2 membrane (3.70%) was much less than that in the PA/UiO-66-NH_2 membrane (59.41%). All of the results showed that PDA interlayer could induce the tight attachment of the PA layer to the support, enhancing the structural stability of TFN membranes. By way of the mechanism of our method, we have further successfully prepared TFN membranes on PES and PAN supports (Fig. S5†), which showed that this strategy can be applied to form versatile TFN membranes using different substrates.

Membrane hydrophilicity has an essential effect on the filtration performance. The hydrophilic properties of the TFC and TFN/UiO-66-NH_2 membranes were characterized by determining their water contact angles (WCAs) (Fig. 9). The improved hydrophilicities of TFN/UiO-66-NH_2 membranes were

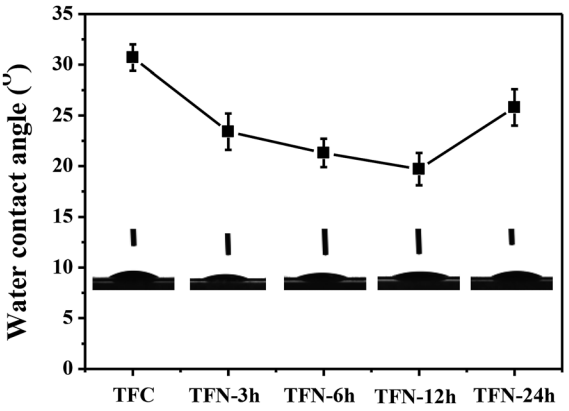

Fig. 9 Water contact angles of TFC and TFN membranes.

confirmed by the reduction of the WCA to 19.7°, when the PDA deposition time was below 12 h. This was most likely attributed to the presence of hydrophilic UiO-66-NH_2, which facilitated superior water wettability to the pure TFC membranes. However, on further increasing the PDA deposition time to 24 h, the WCA of the TFN/UiO-66-NH_2 membrane elevated to 25.8°. The degenerated surface hydrophilicity was likely to result from the rougher nodule-like surface, improving the surface roughness. Furthermore, the nonuniform distribution of UiO-66-NH_2 nanoparticles led to partial aggregation with the increase in PDA deposition time.

The nanofiltration performances of the as-synthesized membranes were evaluated by using self-made cross-flow equipment (Fig. 2). To further understand the effect of PDA modification on the NF performance, the nanofiltration performance of pristine PSF support and PDA-coated PSF membrane was studied. As shown in Fig. S6,† the PWP of PSF membrane decreased with the increase in PDA deposition time and the PWP was maintained at more than 300 L m^{-2} h^{-1} bar^{-1}. At the same time, the Na_2SO_4 and NaCl rejection of the pure PSF support and PDA modified membranes were lower than 2 wt%. All of these results proved that the salts could hardly be rejected by PSF and modified PSF membrane and thus, the salt rejection of TFC and TFN/UiO-66-NH_2 membranes are mainly dependent on the PA dense layers. Compared with the TFC membrane whose pure water permeability (PWP) was 6.3 L m^{-2} h^{-1} bar^{-1}, the PWP of the fabricated TFN/UiO-66-NH_2 membranes increased with the deposition time of PDA, and the highest water permeability reached 13.0 L m^{-2} h^{-1} bar^{-1} at 12 h (Fig. 10a), about 2 times higher than that of commercial NF membranes with similar salt rejection.[37] The significant enhancement in permeability should be largely ascribed to the comparatively loose PA dense layer induced by the incorporation of porous and hydrophilic UiO-66-NH_2 nanoparticles, which provided additional passages for water molecules. Compared to other inorganic nanofillers, MOFs with a PA matrix showed better compatibility and effectively avoided the formation of interface voids such as nonselective defects. Furthermore, UiO-66-NH_2, with –NH_2 functionalized counterparts produced from amino group-containing ligands, provided

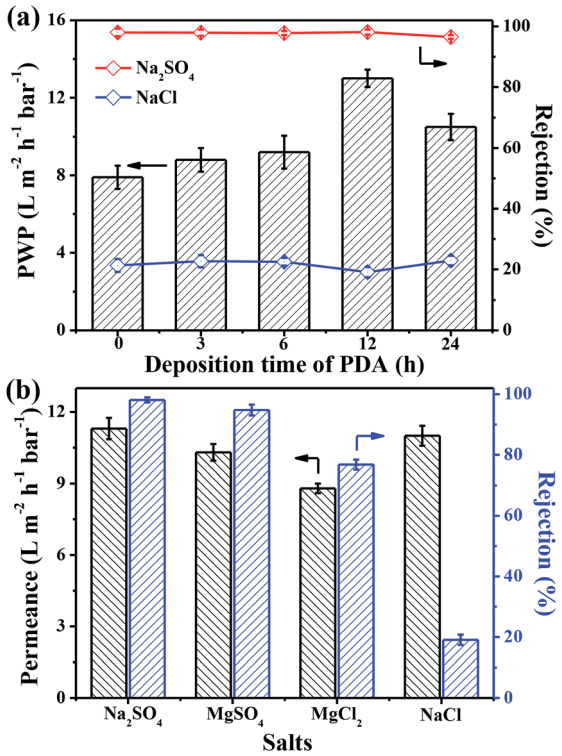

Fig. 10 (a) Change of PWP and salt rejection of TFN membranes *vs.* PDA deposition time. (b) Separation of different salt solutions by prepared NF membrane at optimized condition.

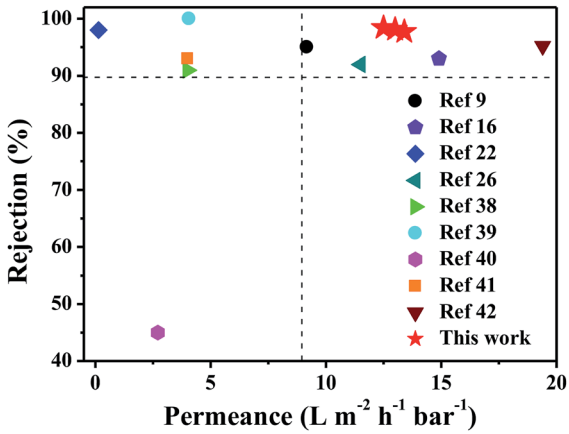

Fig. 11 Comparison of TFN/UiO-66-NH_2 membrane with other MOF-based NF membranes reported (the detailed data are given in Table S1†); values taken from ref. 9, 16, 22, 26 and 38–42.

better interfacial interaction with PA macromolecules, resulting in a great improvement in permeability performance. Moreover, all of the TFN/UiO-66-NH_2 membranes presented excellent retention capability towards Na_2SO_4 (>97%) and much lower retention capability for NaCl (~20%), which indicated that the as-synthesized TFN/UiO-66-NH_2 was a typical nanofiltration membrane. As presented in Fig. 10b, the TFN/UiO-66-NH_2 nanofiltration membrane displayed very high rejection for Na_2SO_4 (98.1%) and the salt rejection followed the order R (Na_2SO_4) > R ($MgSO_4$) > R ($MgCl_2$) > R (NaCl), showing the synergistic effect of molecule sieving and Donnan exclusion. Compared with other MOF-based membranes reported in the literature (Table S1† and Fig. 11), it is evident that our as-prepared TFN/UiO-66-NH_2 membrane displayed extremely high water permeance and very competitive salt rejections for liquid separation.

The amount of nanofillers effectively incorporated into a PA dense layer during interfacial polymerization has a huge impact on the behaviour of TFN membranes. To further investigate the influence of the UiO-66-NH_2 loading, we prepared TFN/UiO-66-NH_2 membranes with different amounts of UiO-66-NH_2 nanoparticles on the PDA-deposited PSF substrates. It was found that the PWP of TFN/UiO-66-NH_2 membranes increased with the loading amount of UiO-66-NH_2, and presented excellent rejection for Na_2SO_4 (Fig. 12). When the loading amount of UiO-66-NH_2 was controlled to as low as 0.01 w/v%, the PWP of TFN/UiO-66-NH_2 membrane can reach 13.0 L m^{-2} h^{-1} bar^{-1}, while for the PA/UiO-66-NH_2 membrane, the PWP was only 7.9 L m^{-2} h^{-1} bar^{-1}. The performance difference between TFN/UiO-66-NH_2 and PA/UiO-66-NH_2 membranes can be attributed to the fact that the distribution of UiO-66-NH_2 in the TFN/UiO-66-NH_2 membrane was better than that in the PA/UiO-66-NH_2 membrane and the loading amount of UiO-66-NH_2 was much higher, which was consistent with the results of PDA@PSF and pure PSF substrates. Specifically, even if the loading amount of UiO-66-NH_2 was minimized to 0.005 w/v%, the PWP of the as-synthesized TFN/UiO-66-NH_2 membrane still maintained a very competitive value of 12.2 L m^{-2} h^{-1} bar^{-1} together with excellent Na_2SO_4 rejection of 97.5%. These results demonstrated that the polydopamine modification strategy could not only offer preferable affinity with polymer binders during interfacial polymerization but also take effective control over the incorporation to minimize the traditional wastage of the costly MOFs, which shows great potential for the large scale production of TFN membranes.

Since membrane stability is a critical characteristic for applications in industry, a long-time test (1440 min) was carried out in a Na_2SO_4 solution at 6 bar to measure the stability of the TFN/UiO-66-NH_2 membrane. As shown in Fig. 13, although

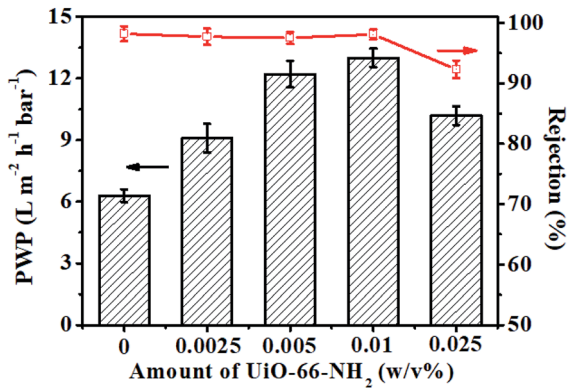

Fig. 12 PWP and Na_2SO_4 retention of TFN/UiO-66-NH_2 membranes with different UiO-66-NH_2 loading.

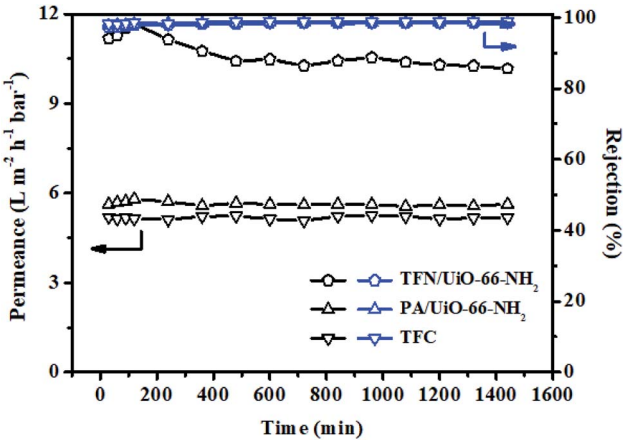

Fig. 13 The permeate flux and rejection changes of TFN/UiO-66-NH_2, PA/UiO-66-NH_2 and TFC membranes during 1440 min NF test. (Test conditions: $P = 6$ bar, $T = 25$ °C and 1 g L^{-1} Na_2SO_4 aqueous solution as feed.)

a slight permeance decrease in the initial stage was observed possibly because of the membrane packing or the concentration polarization on the surface of membrane, which normally happens during nanofiltration, the as-synthesized membranes presented relative stability with regards to both permeability and salt retention capability. For comparison, a batch test experiment (24 h) was carried out to estimate the amount of Zr ion leaching from the synthesized membranes. The ICP results showed that the leaching amount of Zr ion from the PA/UiO-66-NH_2 membrane was about 0.64 ppm during a 24 h operation, while the concentration was reduced to 0.24 ppm from TFN/UiO-66-NH_2, confirming the better stability of the TFN membrane due to strong interactions between UiO-66-NH_2 and the PDA layer, which could be very useful for environmental applications and industrial separation.

Conclusions

In this study, we have proposed a new method to prepare a continuous, well-intergrown and stable TFN/UiO-66-NH_2 membrane for enhanced nanofiltration by using active PDA as a buffering layer. The mediation of PDA coating can help to precisely pre-immobilize nanoparticles and improve the dispersion and anchorage of UiO-66-NH_2 in a PA dense layer, thus greatly enhancing the structural stability of TFN membranes. Moreover, the mutual reaction significantly reduced nanoparticle losses and effectively cut down the actual dosage of UiO-66-NH_2. The fabricated TFN/UiO-66-NH_2 membranes exhibited extremely high water permeance of 13.0 L m^{-2} h^{-1} bar^{-1} and excellent salt rejections of 98.1%, which shows that TFN membranes with controlled nanoparticle incorporation will be promising candidates for environmental applications and industrial separation.

Conflicts of interest

There are no conflicts to declare.

Acknowledgements

We thank for the financial support from the National Natural Science Foundation of China (Grant No. 21736009 and 21476206).

Notes and references

1 R. Zhang, Y. Liu, M. He, Y. Su, X. Zhao, M. Elimelech and Z. Jiang, *Chem. Soc. Rev.*, 2016, **45**, 5888–5924.
2 D. L. Gin and R. D. Noble, *Science*, 2011, **332**, 674–676.
3 Z. Wang, Z. Wang, S. Lin, H. Jin, S. Gao, Y. Zhu and J. Jin, *Nat. Commun.*, 2018, **9**, 2004.
4 R. Zhang, S. L. Ji, N. X. Wang, L. Wang, G. J. Zhang and J. R. Li, *Angew. Chem., Int. Ed.*, 2014, **53**, 9775–9779.
5 Y. H. Chang, Y. D. Shen, D. B. Kong, J. Ning, Z. C. Xiao, J. X. Liang and L. J. Zhi, *RSC Adv.*, 2017, **7**, 2544–2549.
6 F. N. Liu, G. L. Zhang, Q. Meng and H. Z. Zhang, *Chin. J. Chem. Eng.*, 2008, **16**, 441–445.
7 H. Z. Zhang, Z. L. Xu and J. Y. Sun, *RSC Adv.*, 2018, **8**, 29455–29463.
8 Z. Tan, S. F. Chen, X. S. Peng, L. Zhang and C. J. Gao, *Science*, 2018, **360**, 518–521.
9 F. Xiao, B. Wang, X. Y. Hu, S. Nair and Y. B. Chen, *J. Taiwan Inst. Chem. Eng.*, 2018, **83**, 159–167.
10 J. R. Werber, C. O. Osuji and M. Elimelech, *Nat. Rev. Mater.*, 2016, **1**, 16018.
11 H. B. Park, J. Kamcev, L. M. Robeson, M. Elimelech and B. D. Freeman, *Science*, 2017, **356**, eaab0530.
12 R. Z. Pang and K. S. Zhang, *J. Colloid Interface Sci.*, 2018, **510**, 127–132.
13 A. Garcia, Y. Quintero, N. Vicencio, B. Rodriguez, D. Ozturk, E. Mosquera, T. P. Corrales and U. G. Volkmann, *RSC Adv.*, 2016, **6**, 82941–82948.
14 M. R. Mahdavi, M. Delnavaz and V. Vatanpour, *J. Taiwan Inst. Chem. Eng.*, 2017, **75**, 189–198.
15 Q. L. Xie, W. Y. Shao, S. S. Zhang, Z. Hong, Q. Q. Wang and B. R. Zeng, *RSC Adv.*, 2017, **7**, 54898–54910.
16 J. Y. Zhu, L. J. Qin, A. Uliana, J. W. Hou, J. Wang, Y. T. Zhang, X. Li, S. S. Yuan, J. Li, M. M. Tian, J. Y. Lin and B. Van der Bruggen, *ACS Appl. Mater. Interfaces*, 2017, **9**, 1975–1986.
17 H. Furukawa, K. E. Cordova, M. O'Keeffe and O. M. Yaghi, *Science*, 2013, **341**, 1230444.
18 S. Sorribas, P. Gorgojo, C. Tellez, J. Coronas and A. G. Livingston, *J. Am. Chem. Soc.*, 2013, **135**, 15201–15208.
19 W. Li, Y. Zhang, Q. Li and G. Zhang, *Chem. Eng. Sci.*, 2015, **135**, 232–257.
20 C. Van Goethem, R. Verbeke, S. Hermans, R. Bernstein and I. F. J. Vankelecom, *J. Mater. Chem. A*, 2016, **4**, 16368–16376.
21 M. Navarro, J. Benito, L. Paseta, I. Gascon, J. Coronas and C. Tellez, *ACS Appl. Mater. Interfaces*, 2018, **10**, 1278–1287.
22 X. L. Liu, N. K. Demir, Z. T. Wu and K. Li, *J. Am. Chem. Soc.*, 2015, **137**, 6999–7002.
23 D. C. Ma, S. B. Peh, G. Han and S. B. Chen, *ACS Appl. Mater. Interfaces*, 2017, **9**, 7523–7534.
24 C. L. Li, Y. Q. Zhang, M. Yong, W. Liu and J. Q. Wang, *RSC Adv.*, 2019, **9**, 10702–10714.

25 T. Y. Liu, H. G. Yuan, Y. Y. Liu, D. Ren, Y. C. Su and X. Wang, *ACS Nano*, 2018, **12**, 9253–9265.
26 Y. He, Y. P. Tang, D. Ma and T.-S. Chung, *J. Membr. Sci.*, 2017, **541**, 262–270.
27 H.-C. Yang, R. Z. Waldman, M.-B. Wu, J. Hou, L. Chen, S. B. Darling and Z.-K. Xu, *Adv. Funct. Mater.*, 2018, **28**, 1705327.
28 M. M. Zhou, Y. N. Wu, P. P. Luo, J. Q. Lyu, D. R. Mu, A. W. Li, F. T. Li and G. T. Li, *RSC Adv.*, 2017, **7**, 49568–49575.
29 H. Q. Wu, J. M. Ang, J. H. Kong, C. Y. Zhao, Y. H. Du and X. H. Lu, *RSC Adv.*, 2016, **6**, 103390–103398.
30 H. Lee, J. Rho and P. B. Messersmith, *Adv. Mater.*, 2009, **21**, 431–434.
31 H. Yang, Y. Lan, W. Zhu, W. Li, D. Xu, J. Cui, D. Shen and G. Li, *J. Mater. Chem.*, 2012, **22**, 16994–17001.
32 Y. Li, Y. Su, J. Li, X. Zhao, R. Zhang, X. Fan, J. Zhu, Y. Ma, Y. Liu and Z. Jiang, *J. Membr. Sci.*, 2015, **476**, 10–19.
33 C. Zhang, Y. Lv, W. Z. Qin, A. He and Z. K. Xu, *ACS Appl. Mater. Interfaces*, 2017, **9**, 14437–14444.
34 X. Yang, Y. Du, X. Zhang, A. He and Z. K. Xu, *Langmuir*, 2017, **33**, 2318–2324.
35 X. Kong, Z.-L. Qiu, C.-E. Lin, Y.-Z. Song, B.-K. Zhu, L.-P. Zhu and X.-Z. Wei, *J. Mater. Chem. A*, 2017, **5**, 7876–7884.
36 M. Li, Z. W. Lv, J. F. Zheng, J. H. Hu, C. Jiang, M. Ueda, X. Zhang and L. J. Wang, *ACS Sustainable Chemistry & Engineering*, 2017, **5**, 784–792.
37 D. Ren, X.-T. Bi, T.-Y. Liu and X. Wang, *J. Mater. Chem. A*, 2019, **7**, 1849–1860.
38 S. Basu and M. Balakrishnan, *Sep. Purif. Technol.*, 2017, **179**, 118–125.
39 J. Wang, Y. M. Wang, Y. T. Zhang, A. Uliana, J. Y. Zhu, J. D. Liu and B. Van der Bruggen, *ACS Appl. Mater. Interfaces*, 2016, **8**, 25508–25519.
40 L. Y. Wang, M. Q. Fang, J. Liu, J. He, J. D. Li and J. D. Lei, *ACS Appl. Mater. Interfaces*, 2015, **7**, 24082–24093.
41 X. H. Ma, Z. Yang, Z. K. Yao, Z. L. Xu and C. Y. Y. Tang, *J. Membr. Sci.*, 2017, **525**, 269–276.
42 Z. P. Liao, X. F. Fang, J. Xie, Q. Li, D. P. Wang, X. Y. Sun, L. J. Wang and J. S. Li, *ACS Appl. Mater. Interfaces*, 2019, **11**, 5344–5352.